SUSTAINABLE TECHNOLOGY: LASER CLADDING OF BRAKE DISCS REDUCING ITS PARTICULAT MATTER EMISSIONS

TECNOLOGIA SUSTENTÁVEL: RECUPERAÇÃO A LASER DE DISCOS DE FREIO PARA REDUZIR SUAS EMISSÕES DE MATERIAL PARTICULADO

TECNOLOGÍA SOSTENIBLE: RECUBRIMIENTO LÁSER DE DISCOS DE FRENO PARA REDUCIR SUS EMISIONES DE MATERIAL PARTICULADO

PAULO PAIVA O. L. DYER, Dr. | USP – Universidade de São Paulo, Brasil
ANA CLÁUDIA C. DE OLIVEIRA, Dra. | UFLA – Universidade Federal de Lavras, Brasil
CAROLINA HAHN DA SILVEIRA, Dra. | UNIVAP – Universidade do Vale do Paraíba, Brasil
MARIA MARGARETH DA SILVA, Dra. | ITA – Instituto Tecnológico de Aeronáutica, Brasil
GETÚLIO DE VASCONCELOSA, Dr. | USP – Universidade de São Paulo, Brasil

ABSTRACT

The emission of 2.5μm particulate matter (PM2.5) from braking systems poses a significant health hazard. The wear of brake discs contributes to this issue. However, it can be mitigated. In this paper, a brake disk was Nickel laser cladded. Resulting in an improvement of more than 5 times of coefficient of friction and wear resistance. Likewise, under the deduced mathematical model, this improvement brings an estimative of annual reductions of 230,000 metric tons of PM2.5 not emitted; and more than 400,000 deaths, resulting from these emissions, avoided.

KEYWORDS

Sustainability, brake disk, Laser cladding, Matter emissions, PM2.5

RESUMO

A emissão de material particulado de 2,5 μm (PM2,5) dos sistemas de freio representa um risco significativo à saúde. O desgaste dos discos de freio contribui para esse problema. No entanto, ele pode ser atenuado. Neste trabalho, um disco de freio foi revestido com níquel; utilizando laser. O resultado foi uma melhoria de mais de 5 vezes no coeficiente de atrito e na resistência ao desgaste. Da mesma forma, de acordo com o modelo matemático deduzido, essa melhoria traz uma estimativa de redução anual de 230.000 toneladas métricas de PM2,5 não emitidas; e mais de 400.000 mortes, resultantes dessas emissões, evitadas.

PALAVRAS-CHAVE

Sustentabilidade, discos de freio, deposição à laser, Material particulado, MP2,5

http://dx.doi.org/10.29183/2447-3073.MIX2024.v10.n5.141-159
ISSN: 2447-0899 (IMPRESSA) | 2447-3073 (ONLINE)

RESUMEN

La emisión de material particulado de 2,5 µm (PM2,5) de los sistemas de frenos representa un riesgo significativo para la salud. El desgaste de los discos de freno contribuye a este problema. Sin embargo, puede ser atenuado. En este trabajo, un disco de freno fue recubierto con níquel mediante el uso de láser. El resultado fue una mejora de más de 5 veces en el coeficiente de fricción y en la resistencia al desgaste. De la misma manera, según el modelo matemático deducido, esta mejora implica una estimación de reducción anual de 230.000 toneladas métricas de PM2,5 no emitidas, y más de 400.000 muertes evitadas como resultado de estas emisiones.

PALABRAS CLAVE

Sostenibilidad, discos de freno, deposición con láser, material particulado, PM2,5

1. INTRODUCTION

In Brazil and around the world, there has been aggressive urban expansion in the last five decades; expanding land transport (SILVEIRA, 2013). However, this expansion has contributed to the increase in air pollution; and consequently, causing serious damage to health (LARKIN *et al*., 2017; WHO, 2022).

According to research by King's College, although a large portion of atmospheric emissions: gases and particulate matter (PM) originate from mopeds, more than 20% of PM are produced by braking. With the friction between disc and pad releasing fine metallic particles that remain in suspension for long periods. Observing in this way, a problem that goes unnoticed (FUSSEL *et al*., 2022; SELLEY *et al*., 2020).

In this context, researchers have highlighted the importance of utilizing high-technology processes to improve the properties of tools and parts. Increasing its useful life and performance; in view of the working conditions that impose high wear and tear (CALLISTER Jr. and RETHWISCH, 2014). These processes include coating techniques using lasers. In which, a beam of electromagnetic waves (OEM) provides sufficient energy to produce fusion between base metal and coating (VILAR, 1999). As a result, studies indicate that the surface; such as automotive brake discs; could be improved to the point of reducing PM emissions; increasing its useful life and reducing its disposal (SAURABH *et al*., 2023). In which, high-speed laser application techniques (EHLA) prove to be efficient, and feasible in mass production industrial chains (RETTIG *et al*., 2020; OLOFSSON *et al*., 2020). On this topic, recent studies show viable processes for processing brake discs. The results of which are satisfactory in light of the final quality (ARIAS-GONZÁLEZ *et al*., 2016). However, there is still a significant opportunity for research, as these processes exhibit a wide diversity, presenting advantages and disadvantages depending on the typology of the experiment set-up and the use or not of high-speed laser application techniques (ARIAS-GONZÁLEZ *et al*., 2016; SHI *et al*., 2021; TONOLINI *et al*., 2021; SAURABH *et al*., 2023). In this sense, this article presents a new proposal for laser coating of automotive brake discs. Considering EHLA techniques and a rotation system; whose results were analyzed regarding aspects of materials engineering. In a complementary way, the objective was to implement a mathematical model, estimating the reduction in PM depending on the results.

2. CONTEXT

This Chapter will address socio-environmental issues due to the increasing generation of particles smaller than 2.5 microns; or PM2.5 from automotive braking. Next, technological processes for laser coatings will be discussed; which bring technological solutions to the research problem. Finally, the context of the proposed coating technique will be presented.

2.1. Socioenvironmental issue of PM2.5

According to Tiseo (2023), there has been an annual increase in emissions in the last 10 years; culminating in more than 37 billion metric tons emitted in 2022. Of these, according to the latest report from the World Health Organization (2022), 76% are greenhouse gases (CO2, NOX, CH4 and vapors) and the remainder composed by PM2.5. In other words, a solid so fine that it behaves like a gaseous effluent, remaining in suspension for weeks (MENDONÇA *et al*., 2019).

In this way, PM2.5 are transported for kilometers, spreading carcinogenic propensities such as heavy metals that accumulate in the lungs and adipose tissues (MENDONÇA *et al*., 2019; SELLEY *et al*., 2020). Therefore, despite representing 24% of emissions, they are responsible for more than 4 million deaths per year worldwide, as shown in Figure 01. In this sense, it is common to point to mopeds powered by fossil fuels as the biggest emitters of PM2.5; and in fact, these are still the main responsible (SELLEY *et al*., 2020). However, studies show that a significant 20% of the total PM2.5 comes from the braking process of land vehicles; in which the friction between disc and pad releases millions of metric tons per year, or 1 kg/year per disc (FUSSEL *et al*., 2022; SELLEY *et al*., 2020; BONICCI, 2022). Therefore, brake discs are responsible for almost 1 million deaths.

Thus, braking systems are a little-known problem in the context of transport (SELLEY *et al*., 2020). Tonolini *et al*. (2021) explain that the materials/base of these systems present a good cost-benefit ratio.

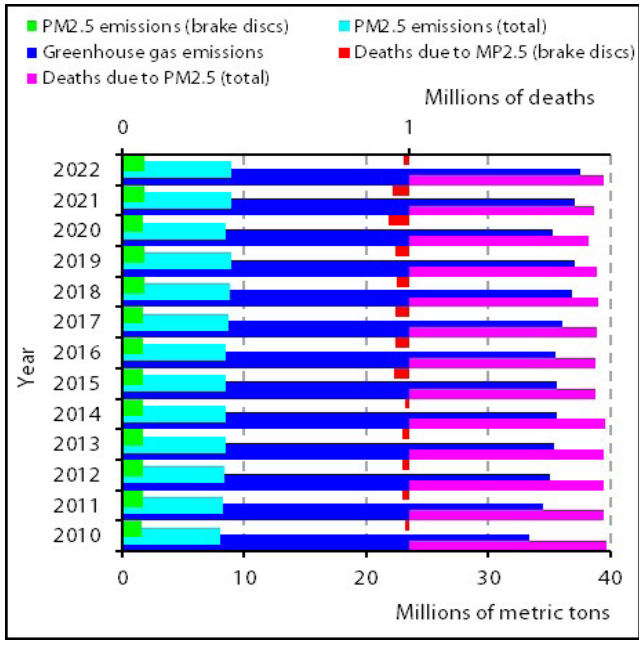

Figure 01: Worldwide evolution of greenhouse gas emissions, PM2.5, and PM2.5-related deaths (brakes and total).

Source: Adapted from Tiseo (2023); WHO (2022); Selley et al. (2020) e Southerland et al. (2022);

Imbued with operability within security criteria; due to good resistance to tension/corrosion and easy workability in casting. Furthermore, Djafri *et al.* (2014) conclude that the porous structure of gray iron (the most used material) provides wear resistance that guarantees coverage over the factory's useful life; which consequently promotes PM2.5 dispersion.

2.2. Laser coating technologies

Callister Jr. and Rethwisch (2014) explain that processing techniques can improve the surface properties of metallic structures, such as tools and parts; highlighting wear resistance and friction coefficient. Thus, starting materials; or substrates; previously fragile and susceptible to wear, they become more resilient due to the structural improvement used on the surface.

In this context, Vilar (1999) highlights the role of laser surface treatments; in which a focused OEM beam reaches temperatures higher than metal melting. Enabling the anchoring of more resistant materials; through metallurgical connections; under the substrate of interest. In contrast, Keist and Palmer (2016) explain that the concentrated OEM is designed with two possibilities of characteristic morphological profiles: Gaussian and Top-Hat; as detailed in Figure 02[A]. In which, Gaussian profiles transfer twice the power in 30% of their profile region. Top-hat beams, on the other hand, provide uniform energy, in theory, throughout the entire trapezoidal cross-section, state Hamburg and Mitra (2012). However, as noted by Tenbrock *et al.* (2020), in many cases there is a central region of diffuse energy, similar to Gaussian profiles; containing peaks with a width smaller than the beam; as also highlighted by Figure 02[A]. Where there is a high energy density, which can produce small cavities in the substrate; depending on the coating method.

Among laser cladding methods, Sommer *et al.* (2021) list directed energy deposition (DED) systems and EHLA extreme speed laser application. According to Li *et al.* (2019), both systems operate with simultaneous laser emission and powder coating injection; in DED the powder is sprayed directly onto the surface of the substrate, while in EHLA, it is injected directly into the focal region of the beam, as illustrated in Figure 2[B]. With this, explain Yong *et al.* (2023), in DED only 20% of the laser energy is transferred to the powder, while in EHLA, this energy is in the order of 60-80%. Increasing the efficiency of EHLA processes, due to its "commitment to transparency", that is, the OEM beam "sees" the substrate without major obstruction. Therefore, the injection of the powder into the focal region promotes its fusion before reaching the molten substrate, as shown in Figure 02[C]. Consequently, the system transfers sufficient energy to provide a satisfactory metallurgical bond between coating and substrate, add Svetlizky *et al.* (2022).

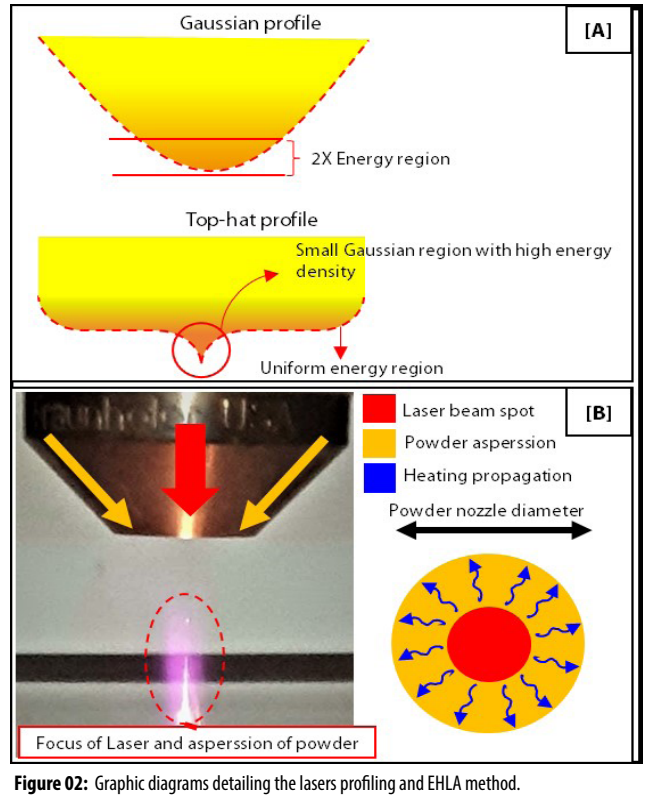

Figure 02: Graphic diagrams detailing the lasers profiling and EHLA method.

Source: Adapted from Homburg and Mitra (2012) and Li et al. (2021);

2.3. Brake disc coating

The application of such processes, such as sustainable technology in brake discs, could significantly contribute to the reduction of PM2.5 due to braking, point out Dyer *et al*. (2024). In fact, as highlighted by Olofsson *et al*. (2020), in addition to reducing PM2.5 emissions, the coating extends the useful life of the disc, impacting the disposal cycle. To this end, the processing parameters must be adjusted depending on the method (DED or EHLA) and beam profile (Gaussian or Top-hat), reinforce Tonolini *et al*. (2021). Considering that the porous nature of gray iron (disc material) can lead to the occurrence of cavities due to vaporization of the surface (ablation) or the occurrence of cracks, due to the effect of expansion, as shown in the micrographs in Figure 3[A] (DYER *et al*., 2024). Likewise, the deposition process must prioritize the uniformity of the coating, depending on the geometry of the disc, highlight Arias-González *et al*. (2016). Noting that each coating line (or "track") must follow the circular design of the surface and be positioned over the neighboring line, with at least 50% of overlay in relation to the width of each track (or "W"); as illustrated by Figure 3[B]. With a powder coating made up of a material that provides improved wear resistance, with good anchoring in the gray iron and with a cost/benefit ratio compatible with the production cost of the disc, add Shi *et al*. (2021).

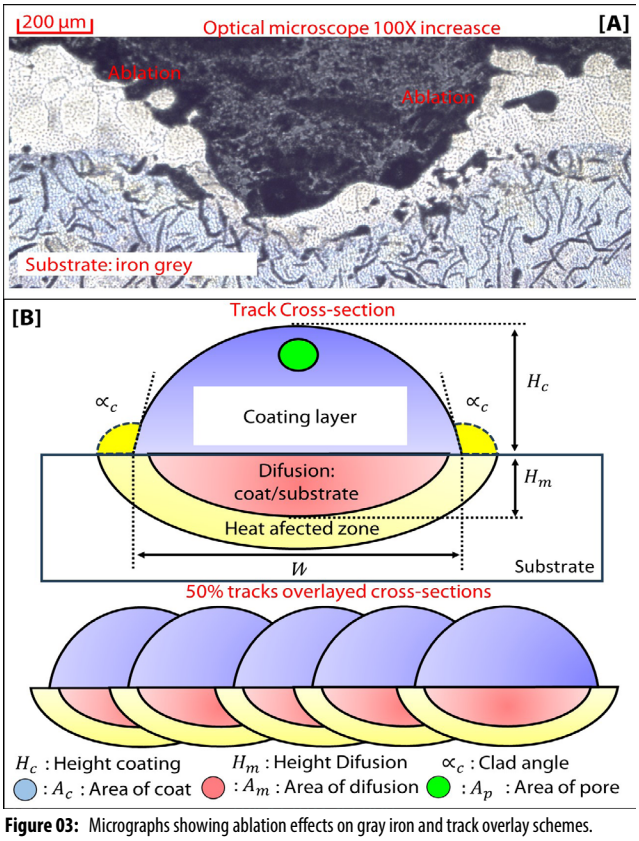

Figure 03: Micrographs showing ablation effects on gray iron and track overlay schemes.
Source: Adapted from: Dyer et al. (2023); Arias-González et al. (2016) e Santos (2017);

In this horizon, Olofsson *et al*. (2020) report the advantages of using a system for rotating the disc during laser deposition. Providing satisfactory uniformity of the coating (Figure 4[A]). Rettig *et al*., (2020) add that using EHLA, with the disc in motion, not only improves the anchoring of the coating, but also reduces processing time (Figure 4[B]); something important from the point of view of application in industrial chains. Hirata *et al*. (2023) in turn, complete that such processes operated by a robotic arm, which carries the laser system and positions the beam through a programming routine, provides precise and efficient execution; reducing adverse effects, such as excessive energy concentrations from Top-hat profiles (ablation and cracks), by the response in real time of the equipment during execution. As a coating, on the other hand, Shi *et al*. (2021) Arias-González *et al*. (2016) highlight the use of Nickel-based alloys; presenting good anchorage in gray iron. Obtaining wear resistance about 1.5 times greater than gray iron. Based on this retrospective analysis, the present study aimed to propose the utilization of technology for sustainable purposes in coating of brake discs. To this end, a method will be proposed consisting of a laser coating system, with disk rotation. In which the emission system is handled by a robotic arm and performs deposition by the EHLA method. At the same time, a mathematical model will be proposed to estimate the reduction in PM2.5 emissions worldwide. Based on increased wear resistance of the disc surface. To this end, results from the microstructural characterization of the material will also be presented, such as wear, friction coefficient, roughness, optical microscopy (OM) and electron microscopy (SEM/EDS).

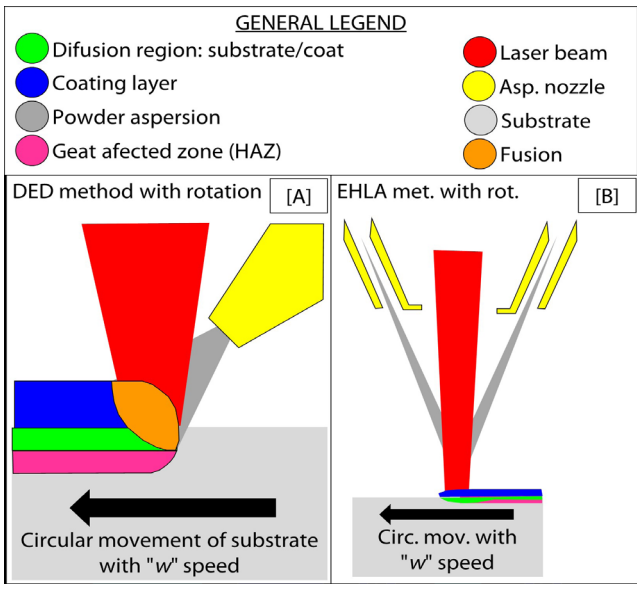

Figure 04: DED and EHLA schemes with disk rotation.
Source: Adapted from: Dyer et al. (2024); Arias-González et al. (2016) e Santos (2017);

3. MATERIALS AND METHODS

To implement technological processes in the service of sustainability, materials, methods and modeling were used. In this experimental development, nickel was laser deposited onto a brake disc. The specimen was evaluated according its mechanical and elemental properties. Likewise, a mathematical model was deduced in order to quantify the PM2.5 not unemitted and deaths avoided resulting of this improvement.

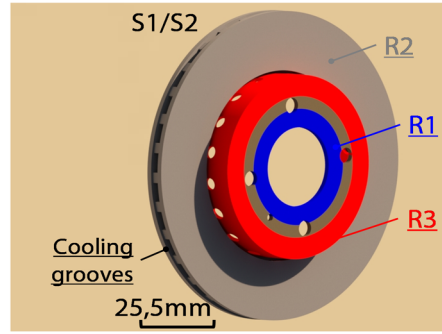

Figure 06: Substrate characteristics.
Source: authors (2024).

3.1 Materials/Equipment

3.1.1 Coating and substrate

As a coating, a commercial Nickel powder (P/M Ni XF Master-Melt PLUS) was used; whose granulometric, morphological and elementary properties (EDS) are presented in Figure 05.

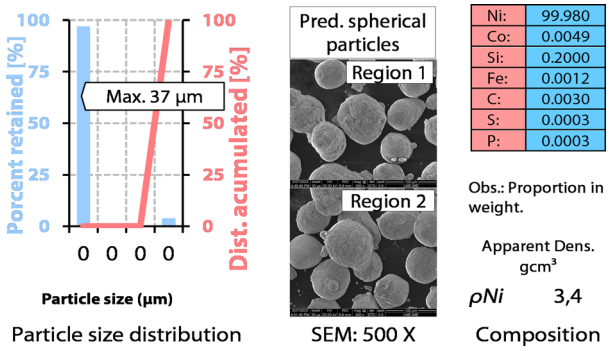

Figure 05: Characteristics of powder coating.
Source: Adapted from: Dyer et al. (2024); Arias-González et al. (2016) e Santos (2017);

According to Figure 05, Ni powder was considered compliant, according to Shi *et al.* (2021). With particles of a homogeneous size of a maximum of 37μm, spherical and little contaminated. As a substrate, were used 2 automotive brake discs (S1 and S2) of specification: "Bd2064" refurbished. With Figure 06 showing discs deposition regions; along with the elementary composition (EDS) of the discs.

According to Rettig *et al.*, (2020), the discs compositions matches that typically found in commercial brake discs; whose design is the most used in passenger vehicles. Therefore, to develop this new coating technique, two experimental setups were realized in order to: 1-Control of parameters and conditions; 2-Coating application and analysis.

3.1.2 Equipment set-up

These set-ups are presented in Figures 07, which also describes the equipment used.

As shown in Figure 07, the coatings were produced by a powder aspersing system; composed of Argon cylinders and a powder feeder (AT-1210 Thermach); Ytterbium fiber laser and head-stock (IPG YLR-1500). Where the laser has λ = 1.07μm and maximum power "*P*" of 1500W; which may be variable at a given efficiency "*E*" (%). The head-stock has a Top-Hat optics beam, with an incidence diameter "b_d" of 6mm. Being "operated" by a Yaskawa GP25 robot; with a payload of 25kg and precision of 100μm, using routines in Phyton language through the RoboDk interface.

According above explanation; this paper aimed to demonstrate a new coating method; by laser cladding; for brake discs in order to reduce PM2.5 emissions.

This system is also equipped with an STC-HD203DV camera; recording (at 10X magnification) the action of the laser. The aspersion system, on the other hand, transports the powder to the focal region of the laser, i.e., like a ELHA method at a certain flow "*st*" of gas (l/min) at a rate "μ" (g /min); depending on the "*Tx*" rotation (RPM) of the perforated disc (100μm in diameter) internal to the feeder, as explained in Figure 08. Where the powder released from the holes in *Tx* falls into the st stream and is aspersed at the μ rate. However, an empirical relationship must be established between [*Tx*, s_t and μ], as will be explained later. At the same time, it is provided a gas supply (without powder); à certain flow "s_g" under the substrate, acting as a surface protective gas.

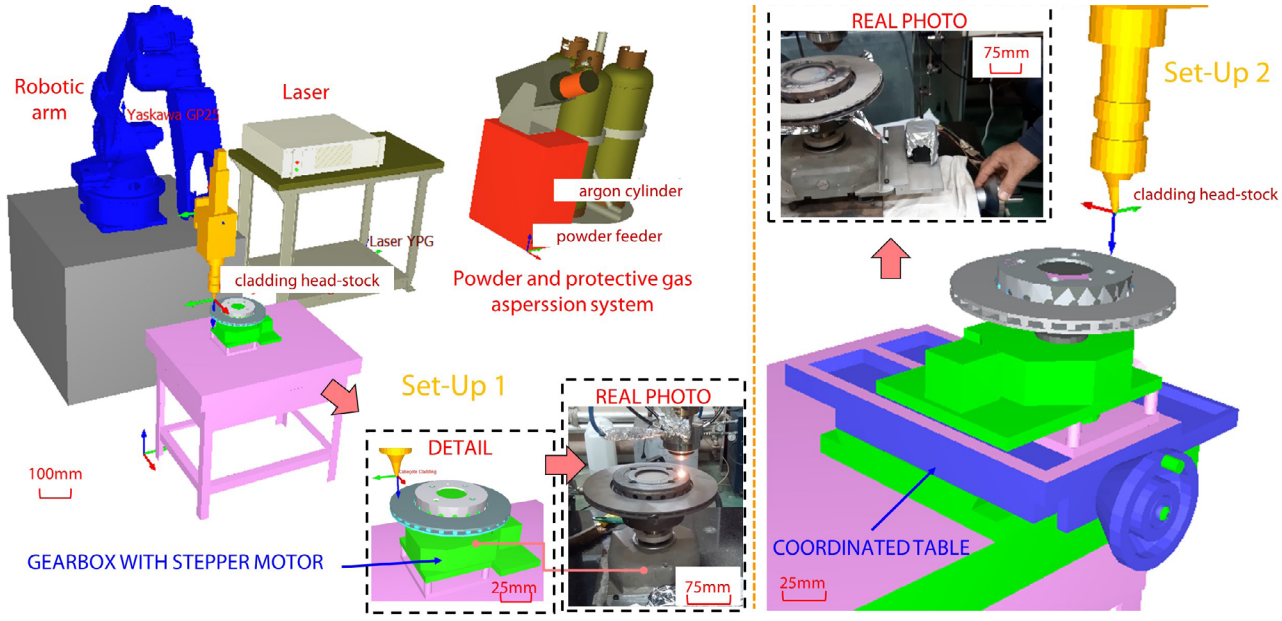

Figure 07: Experimental setups.
Source: authors (2024).

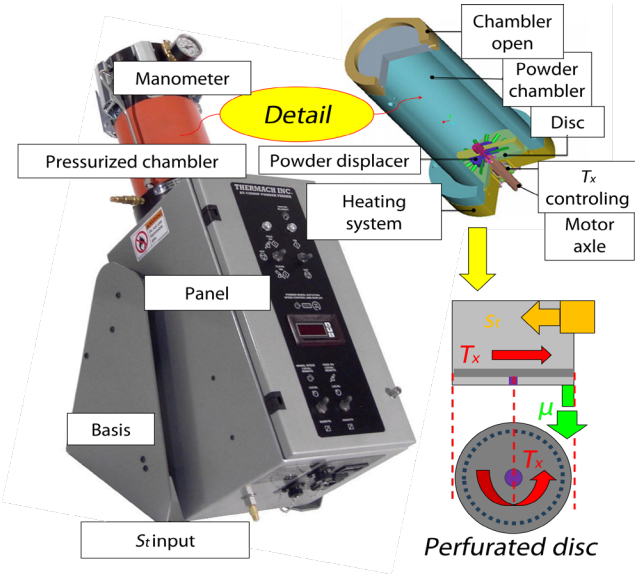

Figure 08: Powder feeder operating diagram.
Source: authors (2024);

For the set-up, S1 and 2 were fixed by a lathe plate (Emco) under a reduction gearbox (National 439), moved by means of pulleys (15 to 48mm) driven by a stepper motor (Steping motor); ensuring a 40X reduction in initial rotation. The operation was carried out by an Arduino system, using G-code (Universal G-code) routines to control the number of turns and angular speeds "ω" (RPM). In set-up 1, this system was mounted on a fixed bench. In set-up 2, this system was placed on a Mr-25 coordinate table.

In the analysis stage, the samples were extracted using diamond discs. Built in Bakelite, with a Buehler insert. Sanded and polished using an Aropol 2V polisher. Analyzed by microscopes: MO - Zeiss and Dino-Lite; and SEM/EDS - Tecsan Vega. Wear and friction were evaluated using Anton Paar TRB^3 and CETR tribometers and Contour X-500 profilometer. To assess roughness, a Taylor Hobson; whose reading was aided by an A-RH Line Tool table to support samples. As well as an FM-700 for Vickers micro hardness (MHV).

3.2 Methods

3.2.1 Initial Stage: Control/conditions

Initially, for experimental, the relationship between *Tx*, st and μ was established; empirically; performing collections, varying st and *Tx*; for a period of time "*t*". Weighing the empty "P_v" and full "P_c" vessel, obtaining the net weight of the powder "P_I" per minute, as a function of st and *Tx*, as shown in the graph of Figure 09; demonstrating the governance of *Tx* over μ.

For the coating, firstly, using S1 in set-up 1, control of tangential speed parameters "v_s" (mm/s) was obtained as a function of the G-code and ω command. In addition to boundary conditions to limit adverse effects on the disc, depending on: *E*, μ and focal length "d_f": which refers to the distance from the head-stock to the substrate. Where, this first step is more detailed in previous work (DYER *et al.*, 2024). To this end, tracks were deposited in S1 with *W* 6mm as concentric circles (R1) and arcs (R2) from within

outward with orthogonal movement of the arm. At E = 70-75% (or 10501125W), μ = 4g/min and st = sg =15l/min. With the G-code command "*F*" varying from 20-300 (RPM), corresponding to the stepper motor rotation (in RPM) which is equivalent to a ω 40X lower. And thus, control of the rotation system was obtained, as well as an optimal range of 9-11mm/s for v_s; allowing the formation of a metallurgical bond between the gray iron and the Ni powder. Then, still in S1, linear tracks were deposited in R3 with the disk stopped to determine boundary conditions. Observing material removal with E > 75% due to energy accumulation and ablations with df < 24mm due to the small Gaussian region of the Top-Hat profile. However, E < 70% and d_f >> 24mm did not anchor Ni. With the definition and control of: F, ω, v_s, E and d_f . In S2; with set-up 1; tracks were deposited in arcs (R2) with v_s = 3-6mm/s, E = 7075% and μ = 4-5.7g/min; observing, through the STC-HD203DV, adverse effects of thermal propagation, depending on the varying thickness of the cooling grooves. Likewise, the variation in the morphology of the molten metal pool as a function of μ was evaluated using the camera. Concluding that the coating for analysis would be carried out in R1, with μ = 4g/min presenting the most homogeneous pool.

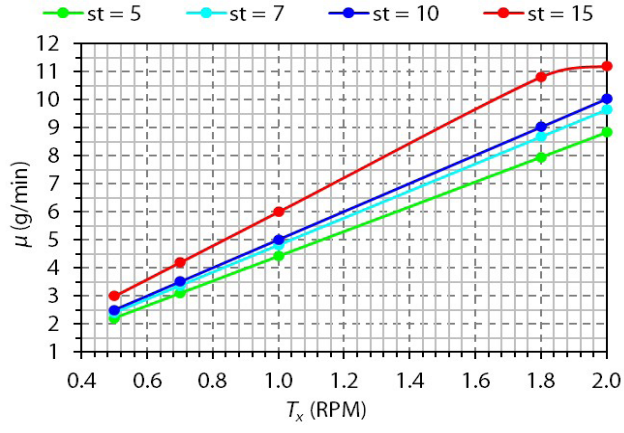

Figure 09: Correlation graph of st, Tx e μ.
Source: authors (2024);

3.2.2. Final Stage: application/analysis

Therefore, S2 was positioned in set-up 2 where circular, concentric tracks were deposited, with W = 600μm, from the inside to the outside on R1 with an "O_v" overlap of 50% for the "*n*" tracks on the entire R1 surface. For this purpose, the arm was kept static; at a d_f = 24mm from S2; varying "d_y" by 300μm by MR-25. Thus, improving coating accuracy. Where the deposition parameters are presented in Table 01. With Figure 10 illustrating this procedure.

Parameters					
variables	**unit**	**value**	**variab.**	**unit**	**value**
E	%	70,00	F	RPM	850
T_x	RPM	0,70	sg	l/min	15
st	l/min	15,00	ω	RPM	21
μ	g/min	4,00	df	mm	24
v_s	mm/s	11,00	n	-	30
O_v	%	50,00	d_y	μm	300
W	μm	600			

Table 1: Laser cladding application parameters.

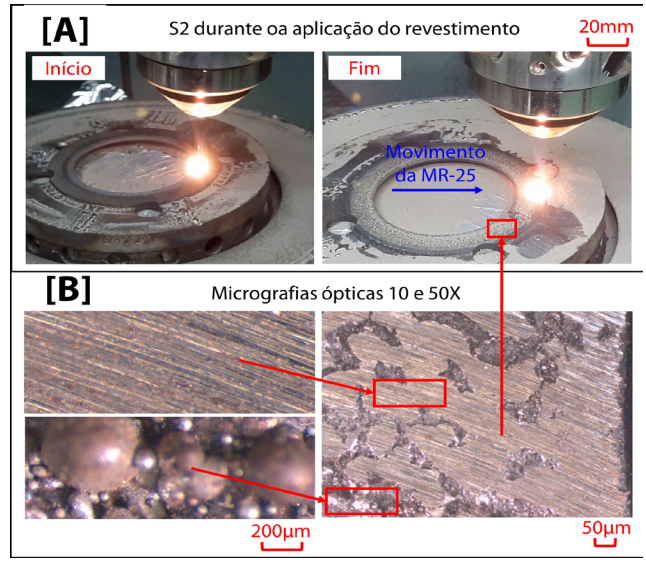

Figure 10: Photographs of the laser deposition process.
Source: authors (2024);

According to Figure 10, the precise movement of MR-25 made it possible a dense and wellconsolidated coating. Which when superficially sanded (Figure 09[B]) revealed a massive and homogeneous surface. Next, both worked surface and cross sections were extracted. After embedding and metallographic preparation, cross section was analyzed by MO (100X magnification). With this, was calculated the dilution "*D*" and coating angle α_c; as Figure's 03 shown; according to Goodarzi's *et al.* (2015) Eqs. 1 and 2. Likewise, this section was SEM analyzed (500X magnification) and EDS mapping.

$$D = A_m\left[A_c - A_p + A_m\right]^{-1} \quad (1)$$

$$\propto_c = 180 - 2\tan^{-1}([2H_c][W]^{-1}) \quad (2)$$

In addition, MHV (100gf, 10s) were also obtained from the sections. In parallel, for surfaces were obtained the friction coefficient "θ" (T^{-1}). In addition, were obtained the

following results: wear coefficient "*K*" (T^{-1}) and wear rate "*k*" (mm^3/N.m).

Where, "k_1"and "K_1" were taken on for surface without coating and "k_2" and "K_2" for surface with coating. To this end, the Table 02 conditions were considered for wear "$K_{[1\ and\ 2]}$" and "$k_{[1\ and\ 2]}$" results calculation.

Likewise, for the roughness test, the "*RA*" value was obtained using parameters also in Table 02. Although, θ and *RA* were obtained directly from equipment output. For $K_{[1\ and\ 2]}$ and $k_{[1\ and\ 2]}$, in the other hand, were used the equations: Eqs 3 and 4 (REYE, 1860; HOLM *et al.*, 1958; SILVA, 2014).

$$K = \frac{(V_e + V_a)}{l_x . N_r} \quad (3)$$

$$k = \frac{(V_e + V_a) HV_m}{l_x . N_r} \quad (4)$$

Where "N_r" is the normal load, "HV_m" is the MHV of the softest material (N/mm^2) and "l_x" (mm) the total distance covered in the test. For roughness test, the needle moves a distance "d_{es}" (mm) with speed "vr_u" (mm/s), as illustrated in Figure 11; which also highlights other variables from these trials.

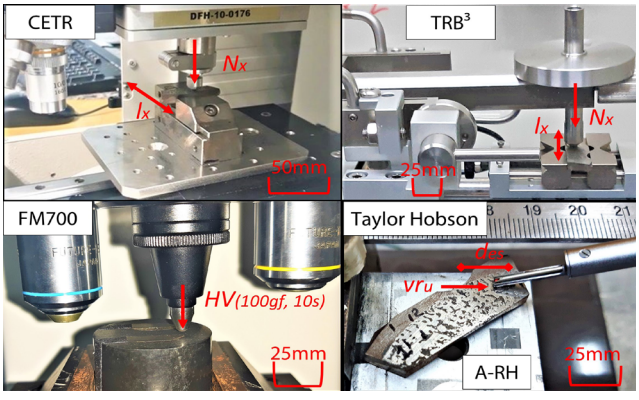

Figure 11: Surface analyses photographs with test conditions.
Source: authors (2024);

Noting that lx is the sum of the total distance traveled by the sphere on the sample surface; with "*Ax*" outward/return amplitude. In addition, "*M1*a" is the initial mass of the sample. Furthermore, "ρ_e", "*HV*e" and "*M1*e" are the corresponding density, hardness and initial mass of the sphere (respectively). For CETR, an A_x of 10mm was measured for 9.6min at 200mm/s. For TRB^3, however, an *Ax* of 2mm was used, traveled back and forth in 400 cycles at 4mm/s.

3.2.3 Mathematical Modelling

The mathematical model deducing stage, was carried out using a structuration based on "methodological routes", according to Dyer *et al.* (2023).

Material Properties					
With coating			**Without Coating**		
var.	un.	valor	var.	un.	valor
ρNi	g/mm³	0,0034	*ρFe*	g/mm³	0,0079
*M1*a	g/mm³	12,827	*M1*a	g	12,827
Wear test - conditions for CETR equipment: radius sphere re = 1,5mm, made by 304 steel					
ρ_e	g/mm³	0,0080	l_x	mm	8400
*M1*e	g	0,2562	N_r	N	5,0
Wear test - conditions for TRB^3 equipment: radius sphere re = 2,5mm, made by 440C steel					
*HV*e	g/mm³	0,0077	l_x	mm	800
*M1*e	g	0,4083	N_r	N	2,0
Roughness test: conditions for Taylor Hobson equipment					

Table 2: Surface analyzes conditions, by equipment.

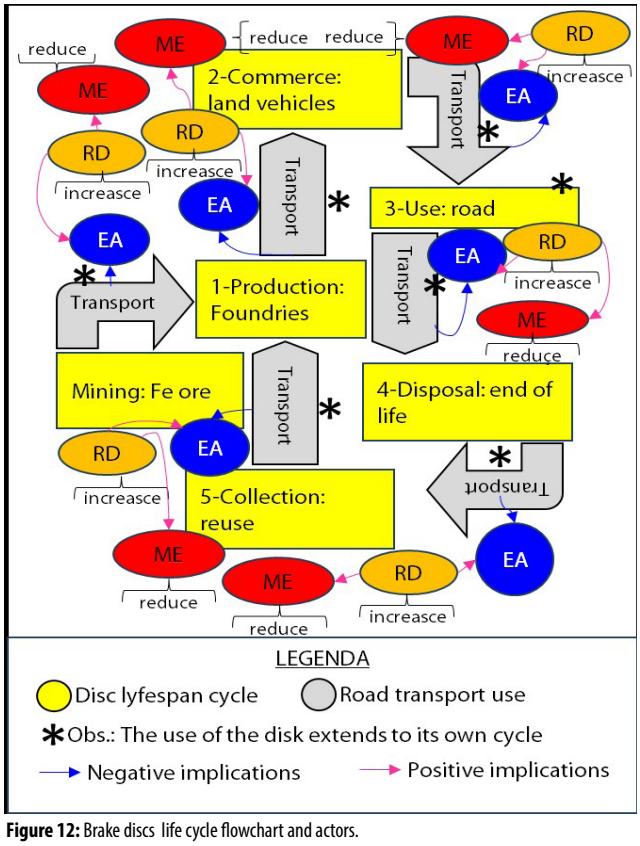

Figure 12: Brake discs life cycle flowchart and actors.
Source: authors (2024);

Firstly, the actors involved were listed. And then, using a methodological route, algebraic variables of interest were named. Finally, boundary conditions were defined.

Considering as input variables: emissions, deaths and reduction in brake disc wear, according to data and Eqs. 3 and 4. According to Bianchi *et al.* (2023), between production and disposal, land transport is used between the stages of the life cycle of brake discs, such The Figure's 12 flowchart shown. Where, the actors were identified: atmospheric emissions (*EA*), deaths due to PM2.5 emissions (*ME*) and positive implications due to wear resistance (*RD*) throughout the cycle.

After listing the actors, functions were structured (Eq. 5) to estimate the reduction in PM2.5 emissions from brake discs (R2.5) and reduction in deaths (*RM*) due to the RD increase factor. Considering that EA covers all pollutants, according to literature. Likewise, the *ME* indices include all deaths (in cases per 100 thousand inhabitants) due to PM2.5 emissions. With this, these indices were broken down, obtaining variables of interest: PM2.5 emissions from brake discs (*ED*) and deaths from PM2.5 (*M2.5*), through the methodological route in Figure 13.

$$R2{,}5 = [ED] - [ED][RD]$$
$$RM = [M2{,}5] - [M2{,}5][RD] \quad (5)$$

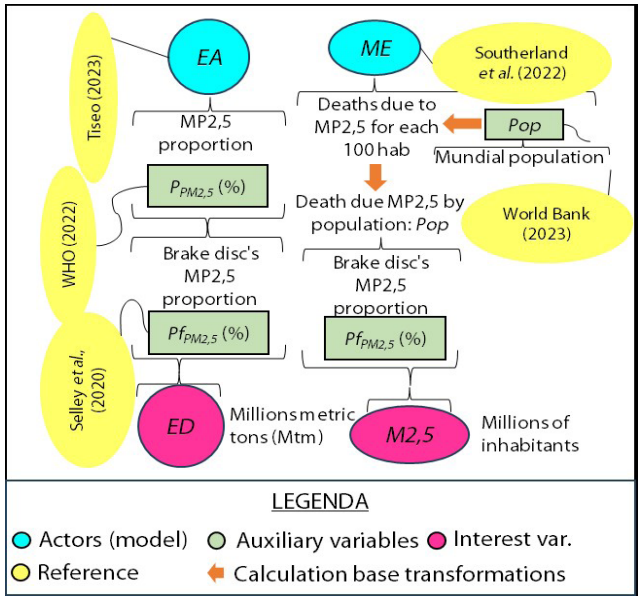

Figure 13: Methodological route for obtaining ED and M2.5.
Source: authors (2024);

From this understanding, were obtained Eq. 6 e 7 for *ED* and *M2,5*; observing the correction factor annual population, in millions of habitants [10^{-12}].

$$ED = [EA][P_{PM2,5}][Pf_{PM2,5}] \quad (6)$$

Next, *RD* was implemented. To this end, unlike EA and ME, this was calculated based on: *k* and *K* (Eq. 3 and 4). According to Figure 14 methodological route; using Eqs. 8 and 9 relative and average difference.

$$Erro\ relativo = [a_1 - a_2][a_1]^{-1} \quad (8)$$

$$Média = [E_1 + E_2][2]^{-1} \quad (9)$$

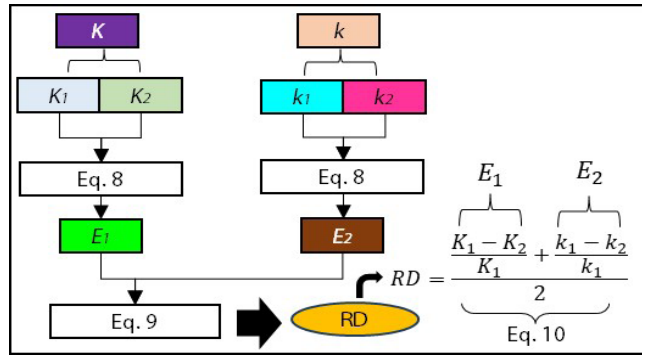

Figure 14: Methodological route for obtaining RD.
Source: authors (2024).

With a_1 and a_2 corresponding to: k_1, k_2, K_1, K_2. Now E_1 and E_2 to the terms K and k respectively. Therefore, at the end of the route, *RD* is dimensionless (Eq. 10), and can act as an absolute proportion factor in Eq. 5.

Replacing *RD* (Eq. 10) and Eqs. 6 and 7 in Eq. 5, the Eq. 11 model was obtained to estimate reduction in emissions and deaths from PM2.5 by brake discs.

$$\begin{cases} R2{,}5 = [EA][P_{PM2,5}][Pf_{PM2,5}](1 - RD) \\ RM = [ME][Pop][Pf_{PM2,5}][10^{-12}](1 - RD) \end{cases} \quad (11)$$

Finally, the boundary conditions were deduced in order to establish maximum and minimum *R2.5* and *RM*. To this end, the "*REM*" ratio in Mtm per %/100 thousand deaths (Eq. 12) was established based on the series of Tiseo (2023) and Southerland *et al.* (2022)

$$REM = [EA][ME]^{-1} \quad (12)$$

Obtaining minimum (*REMa*), average (*REMb*) and maximum (*REMc*) annual *REM*. Then the terms were normalized, as shown in Figure 15. To obtain the range: maximum and minimum *R2.5* and *RM*.

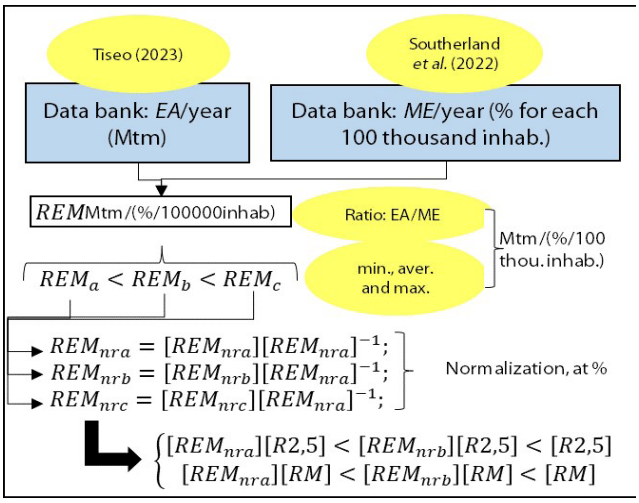

Figure 15: Methodological route for boundary conditions.

Source: authors (2024).

3.3 results

3.4 Cross Section Analysis

The coating layer, composed of multiple tracks, presented microstructure (by MO analysis 50X magnification) with a morphology considered to be of good execution, according to the criteria of Pellizzari *et al.* (2022) for D = 7.5-18.4% and $\alpha_c > 162.3°$, as shown in the micrographs in Figure 16[A]. In this sense, despite the presence of cracks, macro pores and irregularities, mainly in the initial tracks, dense and well-anchored regions were observed (by SEM, 100X magnification) in the substrate. Characterized by the presence of dendritic structures typical of the occurrence of metallurgical bonding (CALLISTER Jr. and RETHWISCH, 2014), as shown in the micrographs in Figure 15[B]; with relative differences: $A_c/[A_p]$ and $A_c/[A_c(\text{expected})]$ within acceptable limits.

Furthermore, the EDS analysis, including total area mapping and specific areas, demonstrated the presence of a mixture of substrate and coating elements in the diffusion region. This confirms the metallurgical bonding, as Figure 17 shown.

The analysis presents accentuated concentrations of Ni and O in the coating region, with a mixture between Ni and Fe in the diffusion region and absence of Ni in the substrate. Proving the metallurgical bond between coating and substrate. The MHV test, in turn, obtained similar results between Ni hardness and gray iron (FC); as shown in Figure 18. Where the two materials have similar hardness and in accordance with the literature (CALLISTER Jr. e RETHWISCH, 2014).

However, Figure 18 shows an increase in hardness in the diffusion zone, characterized by the formation of a metallic alloy between Iron and Nickel. Thus, presenting yet another indication of the formation of a metallurgical bond between substrate and coating.

Figure 16: Morphology of the coated section by MO and SEM.

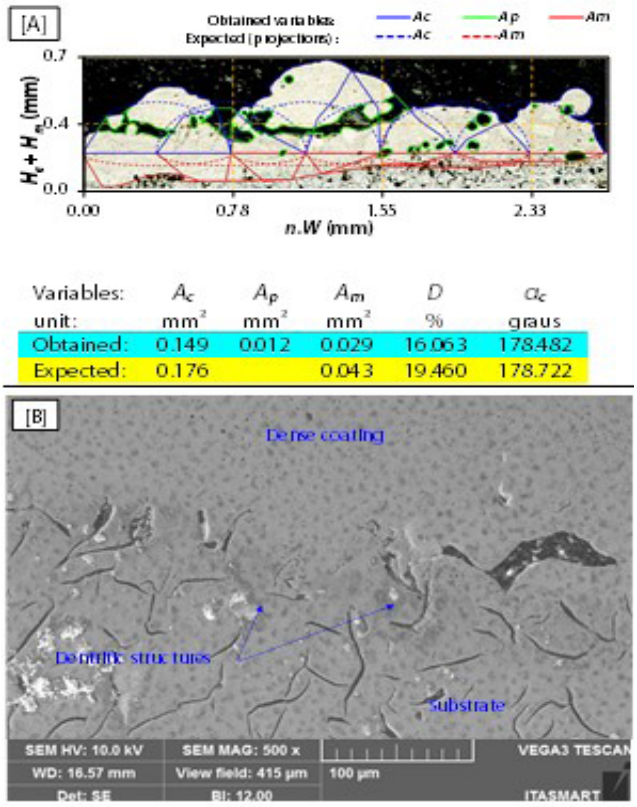

Figure 16: Morphology of the coated section by MO and SEM.

Source: authors (2024).

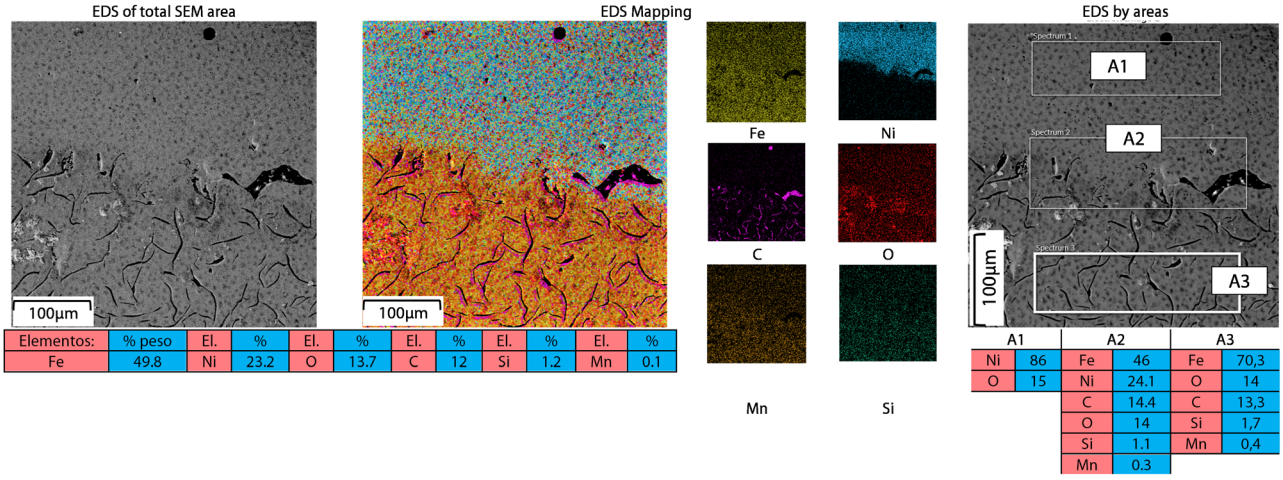

Elementos:	% peso	El.	%	El.	%	El.	%	El.	%	El.	%
Fe	49.8	Ni	23.2	O	13.7	C	12	Si	1.2	Mn	0.1

A1		A2		A3	
Ni	86	Fe	46	Fe	70,3
O	15	Ni	24.1	O	14
		C	14.4	C	13,3
		O	14	Si	1,7
		Si	1.1	Mn	0,4
		Mn	0.3		

Figure 17: EDS of total SEM area, mapping and elemental compositions by areas.
Source: authors (2024).

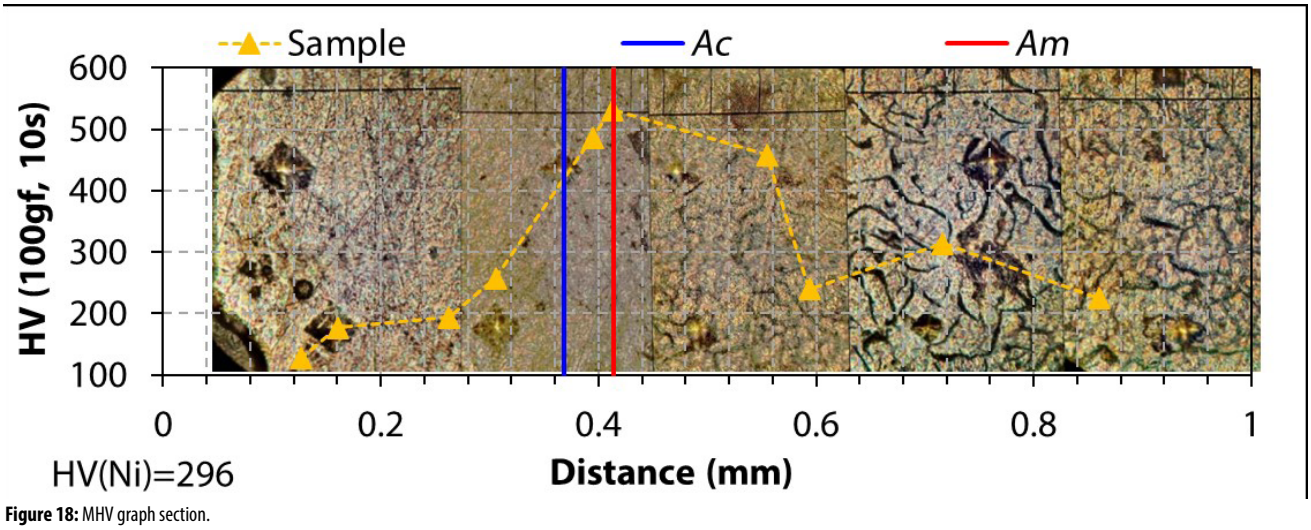

Figure 18: MHV graph section.
Source: authors (2024).

3.5 Surface Analysis

The roughness index "RA" demonstrated that the surface with surface sanding of the coating presented surface characteristics similar to the uncoated disc. Pointed out that the proposal would adapt easily; only with a simple surface treatment; to a conventional braking system, as shown in Figure 19.

Therefore, within an industrial context, the coated discs would only be machined superficially; obtaining the necessary adaptation to the braking system with pad/disc pair. Thus, observing the of industrial application feasibility; with a low economic impact. In addition, the θ coefficients shown a reduction 5 times between coated/uncoated surfaces, as Figure 20 shown. Noting that the alternation of parameters and equipment didn't impact a θ variation. Where, in Figure 20[A], the micrographs (50X magnification) from the Dino-Lite microscope showed darker regions in the uncoated sample; indicating a greater loss of mass. Figure 20[B] (Zeiss, 100X), in the other hand, did not provide much information; due to low visual perception due to the occurrence of macro pores. However, the Countour X-500 confirmed deeper grooves on without coating surfacing (Figure 21[A]) in view of the coated surface (Figure 21[B]).

Therefore, Va was obtained by multiplying the cross-sectional area of the groove "Asa" (mm^2); according to Figure 21[C]; and *Ax*. For Ve, however, "he" was initially calculated by Eq. 13 (cap area) from the groove area "Ase", (mm^2), (Figure 21[D]); being substituted in Eq. 14 (shell volume) to obtain Ve.

With Va and Ve, k and K were calculated for both equipment; despite Figure 21 showing only CETR images (superior visual quality); as shown in Figure 22, comparing

to literature. Where, k and K are superior without coating. Concluding that the disc's Ni coating improved its wear resistance by 3-5 times. Note that there were no major variations in results between equipment; such as to obtain *θ*. However, this gain was almost half that obtained by Tonolini *et al*. (2021); which carried out a similar study. Indicating that there is room for improvement in the technique.

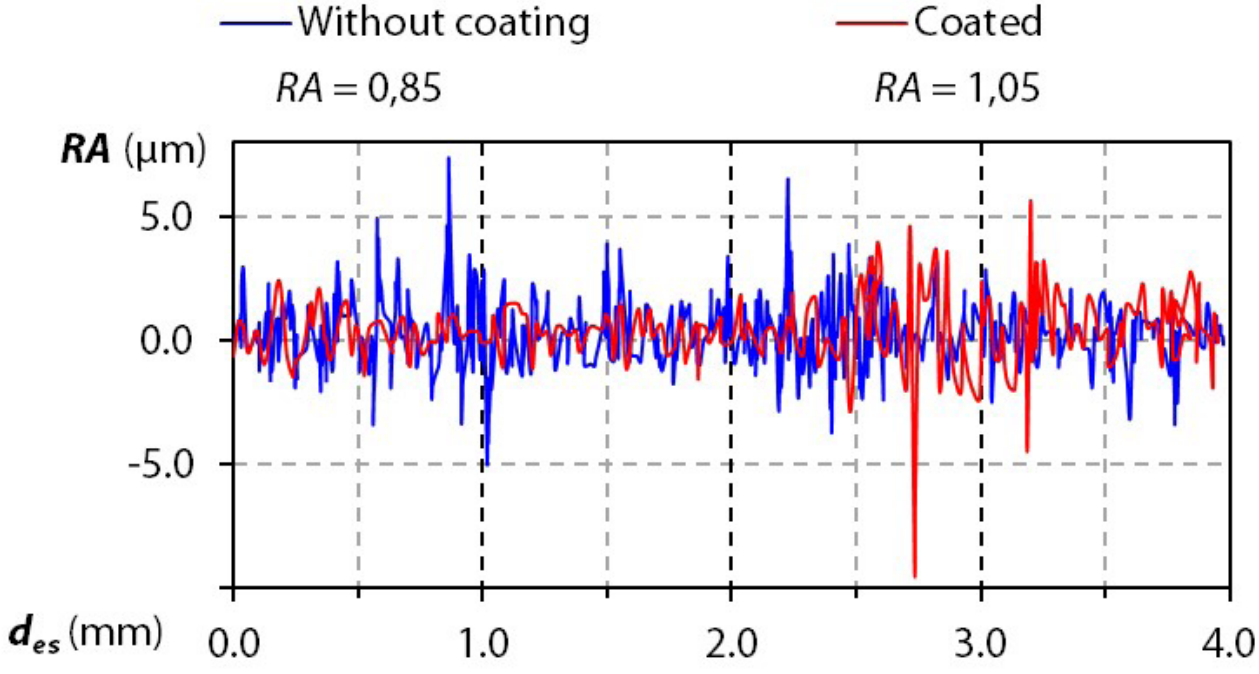

Figure 19: Graph of the roughness test.
Source: authors (2024).

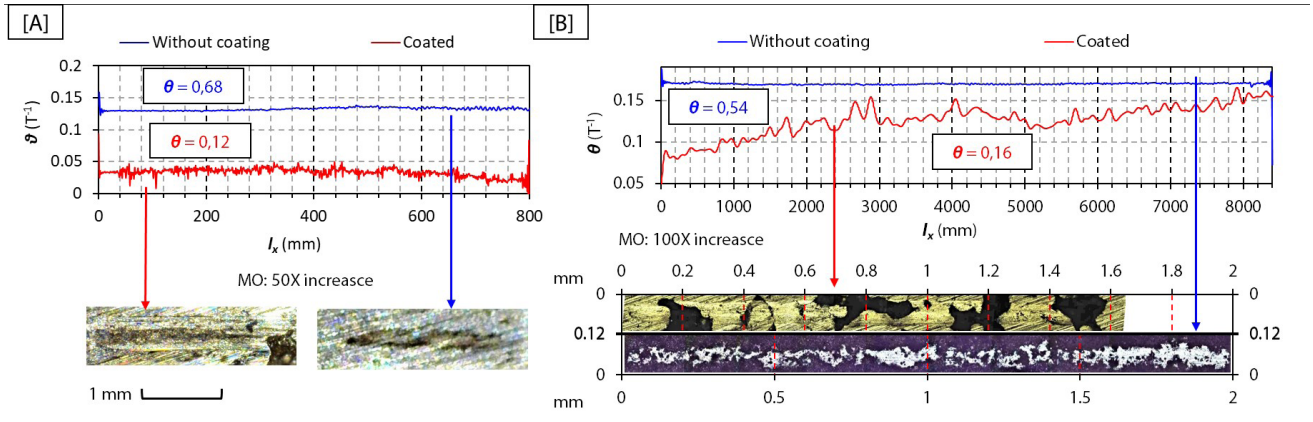

Figure 20: Wear test results for coefficient of friction.
Source: authors (2024).

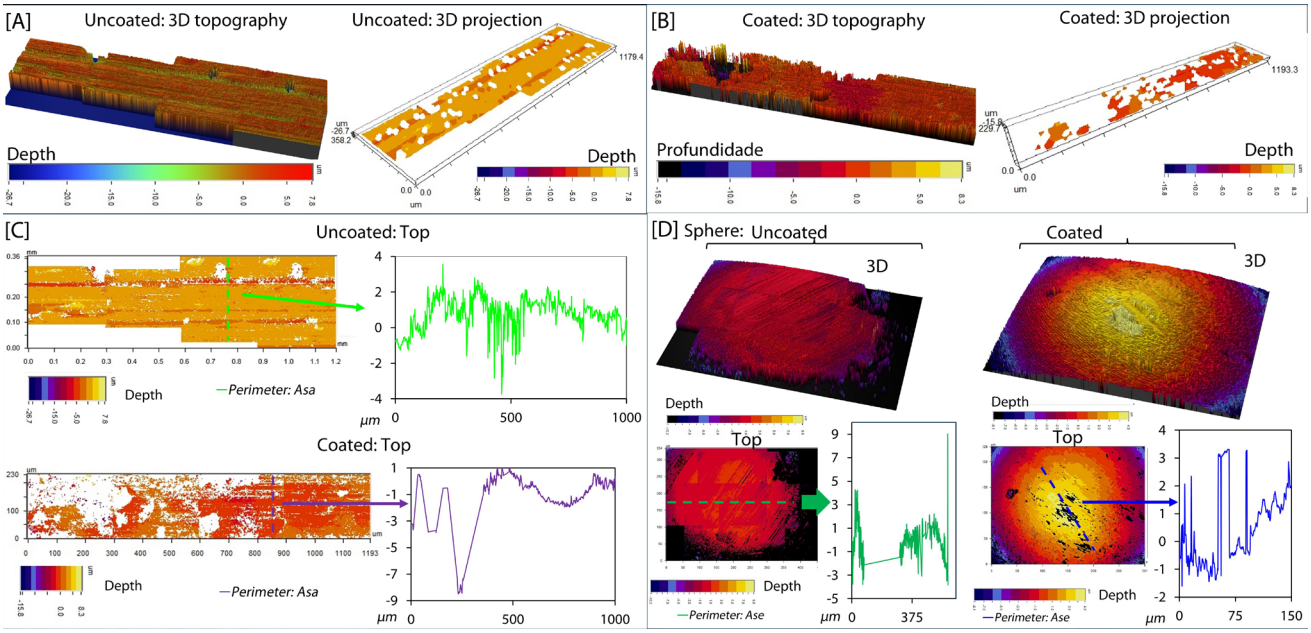

Figure 21: Results of the profilometry test on the CETR equipment.
Source: authors (2024).

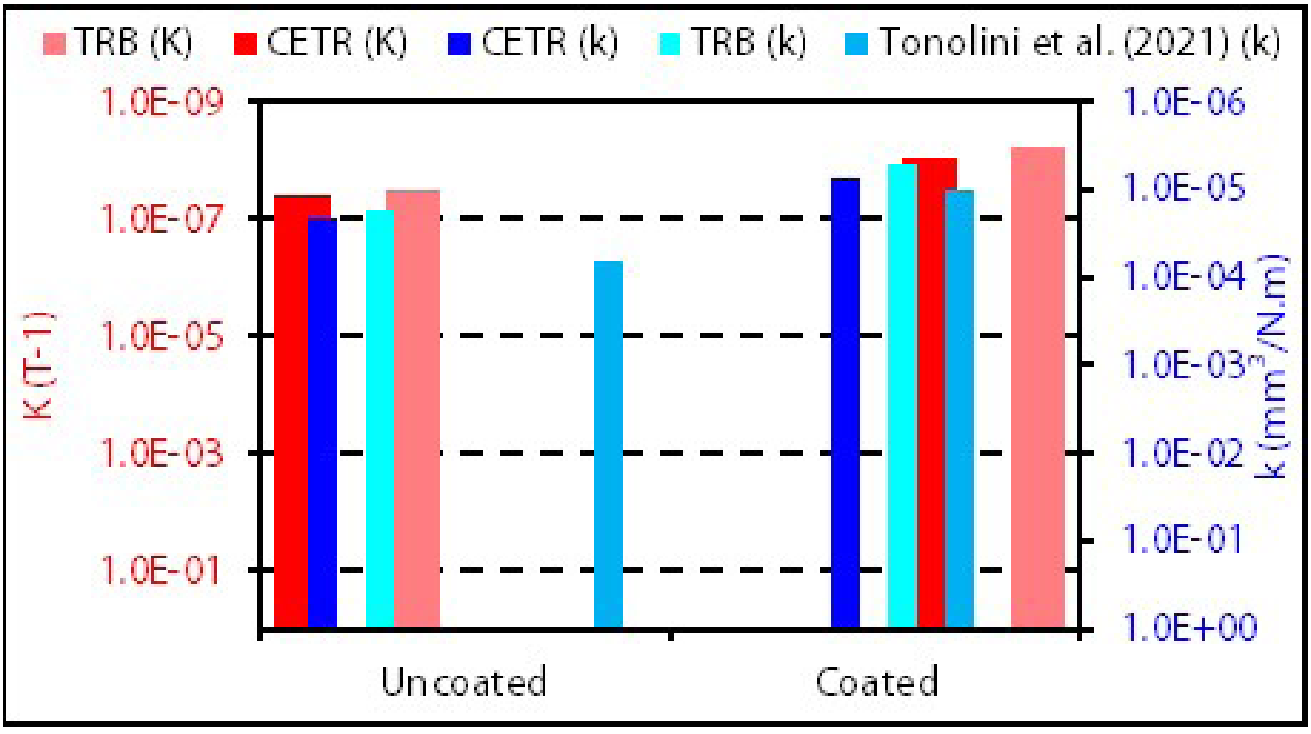

Figure 22: Bar graph with k and K results.
Source: authors (2024).

3.6 Application in the model

The variables: K and k (equipment means), EA and ME (historical series) and Pop (population database) were applied in Eq. 11; estimating annual R2.5 and RM. With annual maximums, averages and minimums being defined (boundary conditions) as Figure 23 graph shown. In addition, Table 03 shown these variables.

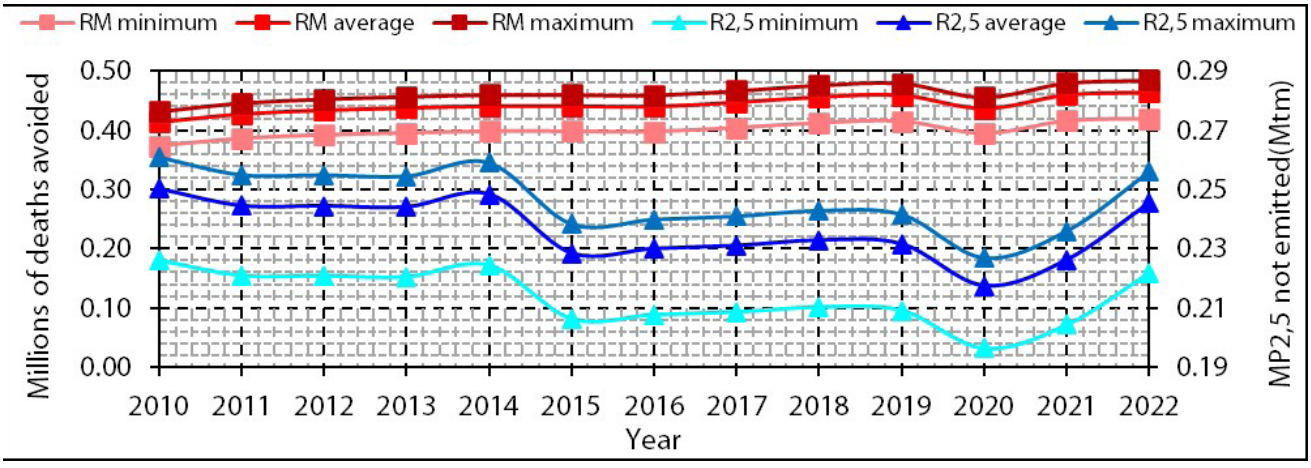

Figure 22: Graph of the benefits obtained with brake disk coating in terms of non-emissions and reduced fatalities.
Source: authors (2024).

Model Variables			
var.	unit	value	reference
PPM2,5	%	24,0	WHO (2022)
PfPM2,5	%	20,0	Selley *et al.* (2020)
K_1	T^{-1}	$3{,}5.10^{-8}$	Average value between CETR and TRB equipment
K_2	T^{-1}	$7{,}6.10^{-9}$	
k_1	$mm^3/N.m$	$2{,}0.10^{-5}$	
k_2	$mm^3/N.m$	$6{,}4.10^{-6}$	

Table 3: Variables applied in Eq. 11 for R2.5 and RM.
Source: authors (2024).

According these results, was observed a reduction of *PM2.5* emission. With this, a significant reduction of deaths was estimated. Thus, highlighting the role of technology in the service of sustainability. In this case, a laser surface treatment process; using Nickel as a coating is capable of preventing the dispersion of 230 thousand metric tons of *PM2.5*, per year on average. Impacting the reduction of more than 400 thousand deaths worldwide; due to respiratory complications.

Obviously, the impact of this processing could not be observed instantly; since the harmful health effects caused by *PM2.5* occur cumulatively. Likewise, the dispersion of this material occurs over the years. However, given such impressive numbers, it can be concluded that improving the wear resistance of automotive brake discs generates positive repercussions in terms of sustainability and population health.

4. CONCLUSION

In conclusion, based on the research problem presented and the proposed mitigation procedures, grounded in relevant literature, it can be affirmed that the objectives of this study were achieved.

Structurally, significant improvements were observed in the brake disc; whose coating morphology remained within the criteria of Pellizzari *et al.* (2022) and similar to the D and α_c parameters observed by Arias-González *et al.* (2016). Regarding mechanical properties, the coefficient of friction stands out, which was almost 5 times lower than uncoated disc and better than other studies: $\theta = 0.43$ (SHI *et al.*, 2021) and $\theta = 0.3$ (TONOLINI *et al.*, 2021).

In the hardness test, on the other hand, despite no improvements occurring; leaving behind other results such as: HV(0.5) = 1060 (TONOLINI *et al.*, 2021); there was additional proof of satisfactory anchoring; as observed by Shi *et al.* (2021) and Arias-González *et al.* (2016). In this case, with similar maximum values: HV(0,3) = 350 and HV(100, 10) = 600, respectively. Where the diffusion region also presented a peak of HV(0,3) = 400 and HV(100, 10) = 600. Proving the occurrence of metallurgical bonding.

Furthermore, an enhancement in the wear resistance of the coated surface was observed, potentially leading to reductions in PM2.5 emissions and associated fatalities, as predicted by the mathematical model implemented in this study. However, compared to other studies, the technique can still be improved in future scopes. Of these improvements, observations noted during the execution of the coatings stand out, such as the implementation of an automated system to reduce errors and improve the uniformity of the tracks Likewise, there is a lack of real-time

control of E to reduce imperfections in the coating such as cracks, macro pores and flaws.

REFERENCES

ARIAS-GONZÁLEZ, F.; VAL, J. D.; COMESAÑA, R.; PENIDE, J.; LUSQUIÑOS, F.; QUINTERO, F.; RIVEIRO, A.; BOUTINGUIZA, M.; POU, J. Fiber laser cladding of nickel-based alloy on cast iron. **Appl. Surf.** Sci., 2015.

BIANCHI, I.; FORCELLESE, A; SIMONCINI, M.; VITA, A.; DELLEDONNE, L.; CASTORANI, V. Life cycle assessment of carbon ceramic matrix composite brake discs containing reclaimed prepreg scraps. **Journal of Cleaner Production**, 2023, v. 413.

BONICCI, D. **How many cars are there in the world? Ever wondered how many cars currently exist in the world and where most ofthem are? Wonder no more.** 23 Apr. 2022, 10:00 AM. Disponível em: https://www.whichcar.com.au/news/how-manycars-are-there-in-the-world. Acesso em: dez/2023.

CALLISTER JR., W. D.; RETHWISCH, D. G. **Materials Science and Engineering an Introduction.** 9. ed. New York: WYLEY, 2010.

DJAFRI, M.; BOUCHETARA, M.; BUSCH, C.; WEBER, S. Effects of humidity and corrosion on the tribological behaviour of the brake disc materials. **Wear,** 2014, v. 321.

DYER, P. P. O. L.; COPPIO, G. J. L.; CIVIDANES, L. DE S.; SILVA, S. A.; SOUSA JR., W. C.; DE LIMA, M. G. A economia na utilização de areia descartada de fundição na construção civil: estudo de caso na cidade de João Pessoa, Paraíba. **Revista Principia - Divulgação Científica e Tecnológica do IFPB,** 2023.

DYER, P. P. O. L.; PAULA, A. DOS S.; HIRATA, A. K.; SANTOS, C. L.; CAMARGO, F. M.; VICENTE, H. DE P.; DOS REIS, J. L.; LE SÉNÉCHAL, N. V.; DE VASCONCELOS, G. DA SILVA, M. M. New parameters evaluation for break disc laser cladding. In: ANAIS DO XXVI ENMC – ENCONTRO NACIONAL DE MODELAGEM COMPUTACIONAL, XIV ECTM – ENCONTRO DE CIÊNCIA E TECNOLOGIA DE MATERIAIS, 25 a 27 de outubro de 2023, 2023. Nova Friburgo. **Anais** [...]. Nova Friburgo: Encontro Nacional de Modelagem Computacional, 2023. Disponível em: https://www.researchgate.net/publication/376073631_NEW_PARAMETERS_EVALUATION_FOR_BREAK_DISC_LASER_CLADDING. Acesso em: Jan/2024.

FULLER, R.; LANDRIGAN, P. J.; BALAKRISHNAN, K.; BATHAN, G.; BOSE-O'REILLY, S.; BRAUER, M.; CARAVANOS, J.; CHILES, T.; COHEN, A.; CORRA, L.; CROPPER, M.; FERRARO, G.; HANNA, J.; HANRAHAN, D.; HU, H.; HUNTER, D.; JANATA, G.; KUPKA, R.; LANPHEAR, B.; LICHTVELD, M.; MARTIN, K.; MUSTAPHA, A.; SANCHEZ-TRIANA, E.; SANDILYA, K.; SCHAEFLI, L.; SHAW, J.; SEDDON, J.; SUK, W.; TÉLLEZ-ROJO, M. M.; YAN, C. Pollution and health: a progress update. **Lancet Planet Health**, 2022, v. 6.

FUSSELL, J.; FRANKLIN, M.; GREEN, D. C.; GUSTAFSSON, M.; HARRISON, R. M.; HICKS, W.; KELLY, F. J.; KISHTA, F.; MILLER, M. R.; MUDWAY, I. S.; OROUMIYEH, F.; SELLEY, L.; WANG, M.; ZHU, Y. A Review of Road Traffic-Derived Non-Exhaust Particles: Emissions, Physicochemical Characteristics, Health Risks, and Mitigation Measures. Environ. Sci. Technol., 2022, v. 56.

GOODARZI, D. M.; PEKKARINEN, J.; SALMINENET, A. Effect of process parameters in laser cladding on substrate melted areas and the substrate melted shape. **Journal of Laser Applications**, 2015, v. 27.

HIRATA, A. K.; SANTOS, C. L.; VICENTE, H. DE P.; DYER, P. P. O. L.; DE VASCONCELOS, G. Thermal effects on metal substrate after irradiation by laser directed energy deposition. In: ANAIS DO XXVI ENMC – ENCONTRO NACIONAL DE MODELAGEM COMPUTACIONAL, XIV ECTM – ENCONTRO DE CIÊNCIA E TECNOLOGIA DE MATERIAIS, 25 a 27 de outubro de 2023, 2023. Nova Friburgo. **Anais** [...]. Nova Friburgo: Encontro Nacional de Modelagem Computacional, 2023.

HOLM, R.; HOLM, E. **Electric Contacts Handbook.** 3. ed. Heidelberg: Springer-Verlag, 1958.

HOMBURG, O., MITRA, T. Gaussian-to-Top-Hat Beam Shaping – An Overview of Parameters, Methods and Applications. In: PROCEEDINGS OF THE LIMO LISSOTSCHENKO MIKROOPTIK GMBH, 4-8., 2012. Bookenburgweg. **Proceedings** [...]. Bookenburgweg Dortmund: Lissotschenko Mikrooptik GmbH Germany, 2012.

KEIST, J. S.; PALMER, T. A. Role of geometry on properties of additively manufactured Ti-6Al-4 V structures fabricated using laser based directed energy deposition. **JMADE,** 2016.

LARKIN, A.; GEDDES, J. A.; MARTIN, R. V.; XIAO, Q.; LIU, Y.; MARSHALL, J. D.; BRAUER, M.; HYSTAD, P. Global Land Use Regression Model for Nitrogen Dioxide Air Pollution. **Environ. Sci. Technol**, 2017.

LI, L.; SHEN, F.; ZHOU, Y.; TAO, W. Comparative study of stainless steel AISI 431 coatings prepared by extreme--high-speed and conventional laser cladding. **Journal of Laser Applications**, v. 31, 2019.

MENDONÇA, T. B.; SATO, L. M.; OGASSAWARA, R. N.; TEIXEIRA, L. R.; ARAGÃO, G. L.; DO SANTOS, G. M.; DE SOUZA, L. S.; MENEZES, C. A. S. Desenvolvimento de um método para análise de partículas de precipitação seca em ambiente atmosférico. **Atas de Saúde Ambiental (São Paulo, online)**, 2019, v. 7.

OLOFSSON, U.; LYU, Y.; ÅSTRÖM, A. H.; WAHLSTRÖM, J.; DIZDAR, S.; NOGUEIRA, A. P. G.; GIALANELLA, S. Laser Cladding Treatment for Refurbishing Disc Brake Rotors: Environmental and Tribological Analysis. **Tribology Letters**, 2021.

PELLIZZARI, M.; ZHAO, Z.; BOSETTI, P.; PERINIET, M. 2022, Optimizing direct laser metal deposition of H13 cladding on CuBe alloy substrate. **Surface & Coatings Technology**, 2022, v. 432.

RETTIG, M.; GROCHOWICZ, J.; KÄSGEN, K.; EATON, R.; WANK, A.; HITZEK, A.; SCHMENGLER, C.; KOß, S.; VOSHAGE, M.; SCHLEIFENBAUM, J. H.; VERPOORT, C.; WEBER, T. Carbidic Brake Rotor Surface Coating Applied by High-Performance Laser-Cladding. In: EURO BRAKE, 2020, Maiz. **Proceedings** […]. Mainz: EuroBrake 2020. International braking technology community & event, 2020.

REYE, K. T. Zur **Theorie der Zapfenreibung:** Der Civilingenieur - Zeitschrift für das Ingenieurwesen, 1860, 6., p. 235–255.

SANTOS, C. L. **Estudo do Processo de Deposição de Stellite 6 com Um Laser de CO2 de 125W.** Tese de Doutorado. São José dos Campos: Instituto Tecnológico de Aeronáutica. Programa de Pós Graduação em Ciência e Tecnologias Espaciais. 2017. 125 p.

SAURABH, A.; VERMA, P. C.; KUMAR, A. Laser Cladding: An Innovative Surface Engineering Technique for Automotive Brake Discs. **Lasers in Engineering (Old City Publishing)**, 2023, v. 55, n. ½.

SELLEY, L.; SCHUSTER, L.; MARBACH, H.; FORSTHUBER, T.; FORBES, B.; GANT, T. W.; SANDSTROM, T.; CAMIÑA, N.; ATHERSUCH, T. J.; MUDWAY, I.; KUMARB, A. Brake dust exposure exacerbates inflammation and transiently compromises phagocytosis in macrophages. **Metallomics**, 2020, v. 12, n. 371.

SHI, X.; WEN, D.; WANG, S.; WANG, G.; ZHANG, M.; LI, J.; XUE, C. Investigation on friction and wear performance of laser cladding Ni-based alloy coating on brake disc. **Optik - International Journal for Light and Electron Optics**, 2021, v. 242.

SILVA, T. P. **Estudo dos efeitos de acumulação de dano por desgaste.** Dissertação de Mestrado. Coimbra: Universidade de Coimbra. Faculdade de Ciências e Tecnologia, Departamento de Engenharia Mecânica. 2014. 41 p.

SILVEIRA, M. R. Infraestruturas e logística de transportes no processo de integração econômica e territorial. **Mercator - Revista de Geografia da UFC**, 2013, v. 12, n. 2.

SOMMER, N.; STREDAK, F.; BÖHM, S. High-Speed Laser Cladding on Thin-Sheet-Substrates-Influence of Process Parameters on Clad Geometry and Dilution. **Coatings**, 2021, v. 11.

SOUTHERLAND, V. A.; BRAUER, M.; MOHEGH, A.; HAMMER, M. S.; VAN DONKELAAR, A.; MARTIN, R. V.; APTE, J. S.; ANENBERG, S. C. Global urban temporal trends in fine particulate matter (PM2·5) and attributable health burdens: estimates from global datasets. **Lancet Planet Health**, 2022, v. 6.

SVETLIZKY, D.; ZHENG, B.; VYATSKIKH, A.; DAS, M.; SUSMITA, B.; BANDYOPADHYAY, A.; SCHOENUNG, J.

M.; LAVERNIA, E. J.; ELIAZET, N. Laser-based directed energy deposition (DED-LB) of advanced materials, **Materials Science & Engineering A**, 2022, v. 840.

TENBROCK, C.; FISCHER, F. G.; WISSENBACHA, K.; SCHLEIFENBAUM, J. H.; WAGENBLAST, P.; MEINERS, W.; WAGNERB, J. Influence of keyhole and conduction mode melting for top-hat shaped beam profiles in laser powder bed fusion. **Journal of Materials Processing Tech.**, 2020, v. 278.

TISEO, I. **Annual carbon dioxide (CO_2) emissions worldwide from 1940 to 2022 (in billion metric tons). STATISTA Data Bank.** Disponível em: https://www.statista.com/statistics/276629/globalco2-emissions/. Acesso em: out/2023.

TONOLINI, P.; MONTESANO, L.; POLA, A.; LANDRIANI, E.; GELFI, M. The effect of lasercladding on the wear behavior of gray cast iron brake disc. **Procedia Structural Integrity**, 2021, v. 33.

VILAR, R. Laser cladding. **Journal of Laser Applications**, 1999, v. 11.

WHO. World Health Organization. World Health Organization ambient air quality database, 2022 update: status report. **IQAir World Air Quality Report**. BISHOP, S. Air Quality Education Specialist. 2020 Research. Clarity. 808 Gilman Street, Berkeley, CA 94710. 2022.

WORLD BANK. **Population estimates and projections. DataBank.** Disponível em: https://databank.worldbank.org/source/populatio n-estimates-and--projections#. Acesso em: dez/2023.

YONG, Z.; CHANG, L.; JIANG, S.; XIE, D.; XING, F.; SHEN, H.; SHEN, L.; TIANET, Z. Parameter optimization of T800 coating fabricated by EHLA based on response surface methodology. **Optics & Laser Technology**, 2023, v. 158.

AUTHORS:

ORCID: 0000-0001-7110-6871
PAULO PAIVA OLIVEIRA LEITE DYER, Doutor em Ciências. Instituto de Estudos Avançados – Departamento de Fotônica, Trevo Coronel Aviador José Alberto Albano do Amarante 01 - Putim, SP, 12228-001. e-mail: paulo_dyer@yahoo.com

ORCID: 0000-0002-2437-8425
Ana Cláudia Costa de Oliveira. Pós-doutorado em Laser Cladding. Universidade Federal de Lavras – Departamento de Engenharia Mecânica Agrícola, Trevo Rotatório Professor Edmir Sá Santos Universidade Federal de, Lavras - MG, 37203-202. e-mail: aclaudiacosta21@gmail.com

ORCID: 0000-0002-4289-7368
CAROLINA HAHN DA SILVEIRA, Doutorado em Química Inorgânica. Universidade do Vale do Paraíba – Instituto de Pesquisa e Desenvolvimento, Av. Shishima Hifumi, 2911 - Urbanova, São José dos Campos - SP, 12244-390. e-mail: cahdsilveira@gmail.com

ORCID: 0000-0002-2356-8198
MARIA MARGARETH DA SILVA, Pós-doutorado em Materiais e Metalurgia. Instituto Tecnológico de Aeronáutica – Departamento de Engenharia de Materiais, Praça Marechal Eduardo Gomes, 50 - Vila das Acácias, São José dos Campos - SP, 12228-900. e-mail: meg@ita.br

ORCID: 0000-0002-2943-0915
GETÚLIO DE VASCONCELOS, Doutor em Ciências. Instituto de Estudos Avançados – Departamento de Fotônica, Trevo Coronel Aviador José Alberto Albano do Amarante 01 - Putim, SP, 12228-001. e-mail: getuliovas@gmail.com

HOW TO CITE THIS ARTICLE:

DYER, P. P. O. L; OLIVEIRA, A. C. C. de; SILVEIRA, C. H. da; SILVA, M. M. da; VASCONCELOS, G. de.Sustainable Technology: Laser cladding of brake discs reducing its particle matter emissions. **MIX Sustentável**, v. 10, n. 5, p.141-159, 2024. ISSN 2447-3073. Disponível em: <http://www.nexos.ufsc.br/index.php/mixsustentavel>. Acesso em: _/_/_. doi: <https://doi.org/10.29183/2447-3073.MIX2024.v10.n5.141-159>.

SUBMITTED ON: 26/04/2024
ACCEPTED ON: 24/09/2024
PUBLISHED ON: 31/11/2024
RESPONSIBLE EDITORS: Lisiane Ilha Librelotto e Paulo Cesar Machado Ferroli

Record of authorship contribution:
CRediT Taxonomy (http://credit.niso.org/)

PPOLD: conceptualization, formal analysis, investigation, methodology, visualization, writing - original draft, writing - review & editing and data curation.

ACCO: formal analysis and writing - review & editing.

CHS: formal analysis and writing - review & edition.

MMS: resources, supervision and writing - review & editing.

GV: project administration, funding acquisition, resources, writing - review & editing, conceptualization and supervision.

Conflict declaration: nothing to declare.